



Study on pulsed wave mode laser welding of Nb-Zr-C alloy and many-objective optimization using meta-heuristic techniques

Santosh Kumar Gupta¹ · Sanjib Jaypuria¹ · Amit Kumar Das² · Dilip Kumar Pratihar² · Partha Saha²

Received: 23 January 2023 / Accepted: 23 August 2023 / Published online: 11 September 2023
© International Institute of Welding 2023

Abstract

Laser welding was carried out in pulsed wave mode to analyze the effect of intermittent heating on the molten-pool thermal history, and metallurgical and mechanical properties of the welded joints of Nb-Zr-C alloy, a prospective structural material for coolant channels in compact high temperature reactors. This study deals with many-objective optimization aiming at improving the mechanical properties of laser welded joint. Duty cycle, welding speed and laser beam diameter were considered as the design variables during the many-objective optimization carried out using traditional composite desirability approach, Bonobo optimizer with weighted sum method and Non-Dominated Sorting Genetic Algorithm (NSGA-III). It led to yield the desirable strength, ductility and hardness properties of the welded joint. Experiments were carried out to validate the suggested optimal parameters obtained using the three techniques. Weighted sum approach combined with Bonobo Optimizer being an intelligent algorithm was able to more closely predict the experimental results compared to other techniques. Welded joint obtained using the energy density of 194.44 J/mm² could yield the highest strength and elongation. Strength and ductility increased with an increase in energy density. Ultimate tensile strength of the optimized welded joint almost matched with that of the base metal. Moreover, a threefold enhancement in micro-hardness value was observed in the welded joint compared to that of the base metal.

Keywords Laser welding · Nb-Zr-C alloy · Mechanical properties · Many-objective optimization · Desirability approach · Bonobo optimizer · NSGA-III

1 Introduction

Fabrication of alloy having application as structural material at high temperature is required to achieve an increase in the operating temperature, which would improve overall efficiency of the nuclear reactors, engines of aviation industry and space craft. Earlier nickel-based alloy was extensively used in the nuclear reactors, aviation industry and engines of spacecraft [1], but the requirement of the improved efficiency and payload by increasing the operating temperature about 1250 °C, entails the need of alloy having high melting point, good weld-ability and formability, resistant to high temperature corrosion, strength at high temperature and resistant to oxidation. Therefore, primary emphasis in the early stages of development was to obtain alloys having high tensile strength at elevated temperature (> 1000 °C), good creep-rupture strength and oxidation resistance. Niobium being a refractory metal has the properties, such as high melting point, corrosion resistant to liquid metals and strength at high temperature [2]. Niobium

Recommended for publication by Commission IV - Power Beam Processes Provided Funding information has to be tagged.

✉ Dilip Kumar Pratihar
dkpra@mech.iitkgp.ac.in

Santosh Kumar Gupta
santoshduce@gmail.com

Sanjib Jaypuria
sanjibjaypuria@gmail.com

Amit Kumar Das
amit.besus@gmail.com

Partha Saha
psaha@mech.iitkgp.ac.in

¹ Advanced Technology Development Centre, Indian Institute of Technology Kharagpur, Kharagpur - 721302, India

² Department of Mechanical Engineering, Indian Institute of Technology Kharagpur, Kharagpur - 721302, India

having low density, easily fabricable, insusceptible to liquid corrosion offered an advantage over other refractory materials like tungsten, molybdenum and tantalum [3]. Niobium-based alloy essentially relied on Tungsten, Molybdenum and Tantalum for strengthening by solid solution to have its application at elevated temperature. Zirconium has low coefficient of thermal expansion and hence, there is very less deformation after welding or change in dimension is minimal in components used in high-temperature applications. However, titanium and zirconium were added to the niobium to improve its oxidation resistance and creep strength. The addition of zirconium should be not be more than 6%, as it increases the diffusion of oxygen near the surface resulting into an increase of hardness [2]. These niobium-based alloys were termed as first-generation alloys. As first-generation alloy, Nb-1Zr was primarily used in the earlier generations of nuclear reactors, but as the operating temperature increased, it was required to further improve the high temperature strength. Carbide was used for precipitation hardening that helped in achieving the required strength [4, 5]. Thus, an alloy of niobium (Nb-Zr-C) was casted, in which a solid solution of niobium and zirconium was further strengthened by carbide addition having an applicability as structural material for temperature range above 1000 °C. Nb-Zr-C alloy has been researched as possible structural material for control rods and heat pipes used in compact high-temperature reactor (CHTR) [6–8].

Niobium and other elements of group V categorized as refractory metals are highly sensitive to contamination by interstitials elements. The resultant effects of contamination can result into catastrophic failure of a structure by degrading the mechanical properties. Hence, high energy welding process in a vacuum operating condition is the suggested technique for niobium-based alloys due to its higher thermal conductivity and melting point. Niobium was used as interlayer to conduct the laser dissimilar welding of Ti alloy and Copper. It was also stated that Nb used as interlayer prevented the mixing of Ti and Cu in the molten pool to avoid formation of any brittle phase [9]. Torkamany et al. [10] attempted pulsed laser welding of Nb and Ti alloy, and the effects of pulse energy, duration and repetition rates were investigated on the melt profile. They also found different phases of Nb and Ti in the weld zone and that might be the cause of degradation of mechanical property. Full penetration welds of Nb-1Zr with optimum bead-geometry, grain structure and mechanical strengths are achieved by electron beam welding (EBW) by holding the beam current fixed at 30 mA. Hardness of the fusion zone (FZ) and heat affected zone (HAZ) zone was found to be significantly lower than the parent alloy. Reduction of tensile strength of the joint was also observed in the optimized 30 mA beam current [11]. The effects of the interstitials, precipitates and secondary alloying elements had been studied for different

niobium-based alloys both at room temperature as well as for the temperature range of 650 °C–900°C [3]. EBW of Nb-1%Zr-0.1%C (PWC-11) having full penetration depth could be obtained by keeping power and scanning speed at high level [12]. Creep testing of welds joined by EBW presented the better strength in comparison to the welds, which were annealed and aged post-welding [13]. Dissimilar EBW of alloy of niobium-hafnium-titanium (C-103) and Ti-6Al-4 V had failure location in fusion zone and grip section of the tensile and fatigue samples, respectively [14]. Bead-on-plate welding of Nb-Zr-C alloy was conducted by laser source and found the different traces of oxygen and nitrogen in the weld, which were migrated from the ambient air during welding. They had suggested a proper shielding technique for conducting laser welding of reactive Nb-Zr-C alloy [4]. However, when the ambient condition exists during welding of these alloys using automated welding head with inert shield of argon and helium in the periphery of fusion zone helps in avoiding the contamination of joints [15, 16]. The niobium alloy, when welded using laser beam welding (LBW) technique, failed in HAZ during uniaxial-tensile tests conducted in normal ambient condition [17].

Laser beam welding of 316 grade of stainless-steel plate with central composite design was conducted to optimize strength, hardness and weld area through desirability approach. Confirmation experiment was also conducted to check the accuracy of the optimized result [18]. The spiking defect in electron beam welds was studied through central composite design-based experimentation. An optimization study had been carried out to minimize the spiking phenomena in these welds through different traditional and metaheuristic approaches. Desirability approach and genetic algorithm (GA) and particle swarm optimization (PSO) tuned weighted sum approach were used to conduct the study and PSO-based weighted sum approach was found to be in superior in terms of predicting the optimized combination. Weighted sum approach is the technique to convert the multi-objective optimization problem into single objective optimization by assigning the weight to individual objective and use them as a whole [19]. Central composite design (CCD) is a statistical approach, which helps in designing the required number of experiments to be carried out. Study on process parameters with respect to the mechanical properties of pulsed laser welded joint had been attempted in this article. CCD was followed for experimentation and response surface methodology (RSM) was used for the parametric study [20]. Jaypuria et al. [21] studied the input–output modelling of electron beam welding through metaheuristics-tuned neural network and found the metaheuristic approaches to be effective in modelling the process in addition to optimizing it. Response surface methodology along with central composite design were applied for the laser welding to develop prediction model of the responses. The

developed model had good consistency between experimental and predicted results [22]. The input–output modelling of hybrid laser welding was conducted by following the central composite design experimentation, which is the statistical alternative to reduce the replication and cost associated with full-factorial design [23]. Here the authors discussed and compared the prediction capability of metaheuristic tuned algorithm in laser welding and found that particle swarm tuned algorithm found to be superior as compared genetic algorithm-based model. The local and global search capability of PSO made the algorithm more suitable for prediction [24]. Bonobo and other two swarm-based algorithms were used for optimizing the mechanical properties of electron beam welded copper alloy and the bonobo optimizer (BO) was found to be effective in predicting the optimized process parameters' combination. The proper balance of selection pressure and population diversity in the BO algorithm through fission–fusion social behaviour make it an efficient algorithm [25].

If the number of objectives becomes more than three, the many-objectives optimization comes into play and for this, a few metaheuristics approaches have been developed in the recent past. The use of these algorithms is more beneficial in handling the individual objective of the response [26]. Multi-objective optimization problem was solved to obtain desirable properties using mathematical equations. Input parameters were optimized to obtain strength, ductility [27] using multi-objective genetic algorithm. Mass removal rate, roundness error and mean diameter-to-height ratio were the output characteristics for electro-jet drilling, that was optimized using grey relation analysis [28]. Dilution in laser cladding was optimized to ensure proper bonding and desired clad bulk property [29]. One of the recent and popular algorithms is NSGA-III [30], which was widely used to solve various engineering problems. Response surface methodology along with NSGA-II was used to optimize the multi-objectives of laser biological tissue welding. The optimized results led to maximum bonding strength and peak temperature of the tissue in this study [31]. Hybrid laser arc welding was optimized by NSGA III to maximize the depth of penetration and tensile strength. The Pareto-front obtained from the NSGA III demonstrated efficiently many solutions to improve the responses as required [32].

In the present study, double sided inert gas shielded pulsed laser welding of Nb-Zr-C was attempted. Analytical study for the selection of optimum process parameters for laser welding of reactive niobium-based alloy is limited, and hence, a systematic study using modern optimization technique is required for deciding the set of input parameters to obtain desirable mechanical and metallurgical properties. In this study, tensile strength, yield strength, ductility and hardness of the welded joints were considered as response variables, while the duty cycle (D.C.), scanning

Table 1 Chemical composition of alloy in weight percentage

Element	C	Zr	Ta	Fe	Nb
wt. %	0.06	0.77	0.03	0.30	Balance

Table 2 Properties of parent metal

Hardness (VHN)	Y.S (MPa)	U.T.S (MPa)	EL (mm)
108.0	251.6	375.1	11.1

speed (S) and beam diameter (D) were regarded as process variables. These four objectives of the study were optimized using traditional composite desirability approach, recently developed Bonobo algorithm with weighted sum approach and a many-objective optimization algorithm, namely, NSGA-III. In addition to this, metallurgical studies, that is, Scanning Electron Microscope (SEM), Energy-dispersive X-ray spectroscopy (EDAX) and X-Ray diffraction analysis (XRD) analyses were used to correlate the microstructure and phases of fusion zone with the mechanical properties of the joints. Additionally, molten pool behavior (cooling rate, peak temperature and molten pool life time) of the pulsed laser welded Nb-Zr-C alloy was studied to establish the relations among energy density and different aspects of grain refinement and associated mechanical behavior of the joint. A confirmation study for the suggested results obtained using the algorithms was also conducted to identify the suitable algorithm with minimum deviation from the predicted values.

2 Material and methods

2.1 Materials

Nb-Zr-C alloy was characterized using X-ray fluorescence (XRF) and carbon–sulphur analyzer (G4-ICARUS) to quantify the weight percent of the alloying elements. The composition and mechanical properties of the alloy has been detailed in Table 1 and 2.

2.2 Experimental procedure

The parent metal of 0.5 mm thickness was cut to 35 × 20 mm dimensions using wire electrical discharge machine (WEDM) followed by edge preparation and cleaning, which includes removal of oxide layers from each surface. Light etching in the solution of HF, H₂O, H₂SO₄ and HNO₃ (mixed in the ratio of 22:55:15:8) and ultrasonic cleaning with propanol had been done to remove impurities that can deteriorate material properties during the welding. Cleaned sheets

were then clamped on the both sides and provision for argon shielding was made on the top and bottom of the sheets at the joining interface. The argon flow was maintained at 5 L/min to avoid contamination of FZ by atmospheric gases, such as oxygen, nitrogen and hydrogen [7]. Laser welding had been performed in butt configuration using Yb-fiber laser (IPG YLR-2000), having an operational wavelength of 1.064 μm with 2 kW maximum output power. Laser focal length was kept fixed to 200 mm during the experiment, and spot diameter had been varied by adjusting stand-off distance. Pyrometer was used to capture the molten-pool's thermal history, which helped in the calculation of cooling rate. Figure 1 shows the experimental setup of the laser welding used for this work. Duty cycle, welding speed and beam diameter were considered as the analytical input parameters in the laser welding. Variation in these parameters affects the micro-hardness, yield strength, ultimate tensile strength and elongation. To optimize these parameters, three levels of selected input parameters were taken in the present study. The levels for each parameter have been shown in Table 3.

2.3 Characterization process

The mechanical and metallurgical properties were analyzed to study the effect of the input parameters on the welded sheets. The characteristics of the welded samples were studied by considering the micro-hardness, yield strength, ultimate tensile strength and elongation. The weld characteristics were also compared to the parent metal. The welded joints were sectioned along weld cross-section using WEDM for metallographic analysis. The sectioned part was polished and then, etched using a solution of HF, H₂SO₄ and HNO₃ mixed in the ratio of 1:3:1. Micro-hardness of the FZ, HAZ and base metal was determined using OMNITECH MVH-S-AUTO machine with load maintained at 50 gm and dwell time was kept equal to 10 seconds. Optical microscope and

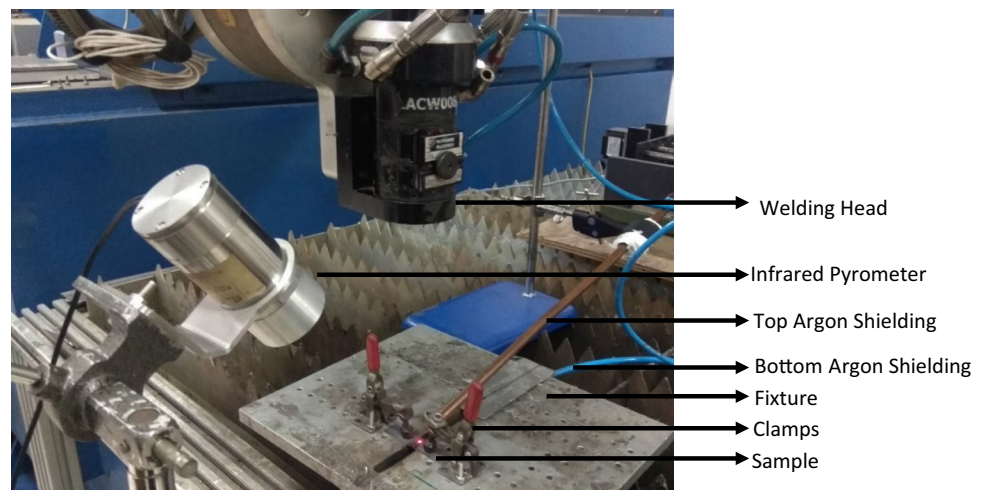
Table 3 Input process parameters for laser welding of Nb-Zr-C alloy

Input parameters	Symbol	Lower Level	Upper Level
Duty Cycle (%)	D.C.	50	70
Welding Speed (mm/min)	S	600	1000
Beam Diameter (mm)	D	0.66	0.82

SEM coupled with EDAX was used for studying the grain morphology, micro features and to quantify the elemental variations in the BM, FZ and HAZ. X-ray diffractometer manufactured by PANalytic Empyrean generating Cu K α radiation were the mask and divergence size was 5 mm and 3 mm. Counting time and step size was held constant at 293.50 s and 0.052 for the measurement. The phase identification was carried out by maintaining the voltage and current at 45 kV and 40 mA respectively. The Uni-axial strength was measured using INSTRON 5500 with a cross head speed of 0.2 mm/min. The tensile specimens were cut using WEDM by following ASTM E8 standard. The sample was sub-sized and depicted in the Fig. 2. A comparison study was carried out based on mechanical and metallurgical properties of (a) base metal, (b) weld with optimized input parameters, (c) weld with high micro-hardness and low strength and ductility, (d) weld with low micro-hardness and high strength and ductility. Pyrometer was used to record molten pool life-time of the welding experiments. The data of the welding experiment were optimized using meta-heuristic optimization techniques and then, confirmation test was done by carrying out the welding experiments using the optimized input parameters.

The welding experiments were carried out by following central composite design (CCD) with 3 centre points (as given in Table 4). The center points enable us to achieve precision in the results by replication. A total of 17 set of experimental combination was conducted according to the

Fig. 1 Experimental setup for laser welding



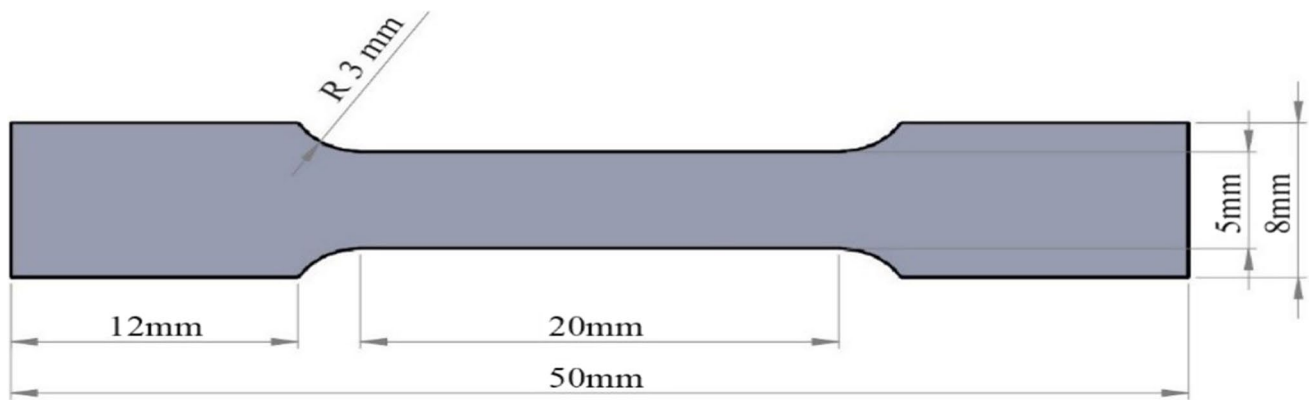


Fig. 2 Tensile specimen for uni-axial test

Table 4 Central Composite Design for laser welding of Nb-Zr-C alloy with corresponding output values

Sl No	Input process parameters				Outputs			
	Duty Cycle (D.C.) (%)	Welding Speed (S) (mm/min)	Beam diameter (D) (mm)	Energy density (J/mm ²)	Hardness (VHN)	Y.S (MPa)	U.T.S (MPa)	EL (mm)
1	50	600	0.72	138.88	381.1	205.9	371.3	7.1
2	70	600	0.72	194.44	378.8	210.1	360.6	7.9
3	50	600	0.82	121.95	388.1	212.8	371.9	7.1
4	70	600	0.82	170.73	370.3	216.6	360.7	7.7
5	60	600	0.66	181.81	378.4	212.4	351.9	6.8
6	50	800	0.66	113.63	410.5	206.3	306.4	3.3
7	60	800	0.66	136.36	390.4	209.6	322.4	5.4
8	60	800	0.66	136.36	394.9	204.5	324.8	5.3
9	60	800	0.66	136.36	390.7	210.1	325.2	5.4
10	70	800	0.66	159.09	386.3	210.4	351.7	6.2
11	60	800	0.72	125.00	396.7	206.8	324.9	5.2
12	60	800	0.82	109.75	383.4	206.1	323.3	5.4
13	60	1000	0.66	109.09	413.8	203.6	301.6	3.6
14	50	1000	0.72	83.33	424.5	202.6	293.2	3.8
15	70	1000	0.72	116.66	403.1	207.5	312.3	4.8
16	50	1000	0.82	73.17	426.7	202.3	304.4	3.3
17	70	1000	0.82	102.43	406.4	208.1	315.7	5.1

response surface method. The experiments as tabulated were carried out thrice for each combination of input parameters to check the agreement of the result of each individual run. The output data presented in the Table 4 are the average calculated value corresponding to each experimental run.

3 Tools and techniques used for optimization

In this study, three different algorithms, such as traditional composite desirability approach (CDA), recently-proposed Bonobo Optimizer (BO), and Non-Dominated Sorting

Genetic Algorithm (NSGA-III) had been implemented to solve the optimization problem of interests. Here, the brief descriptions of the algorithms BO and NSGA-III are given below.

3.1 Brief description of BO

Recently, an intelligent and adaptive metaheuristic technique, named as Bonobo optimizer (BO) [33] was proposed in the literature. It was designed based on the lifestyle and mating strategies of Bonobos. Similar to a few other animals, like Chimpanzees, Elephants, etc., Bonobos are also found to follow the fission–fusion type of social-behavior. In this

type of social-style, Bonobos are observed to form several small parties with varying sizes and compositions and they roam about their living places for doing various activities, like exploring new food sources, safe places for staying, etc. This process is termed as fission. After a certain period of time, they again reassemble (fusion) to serve some specific purposes, such as sleeping together at night, combined attacking against the rivals, etc. This adopted lifestyle of fission–fusion helps Bonobos to find out new food sources and other living-requirements, efficiently. Besides this, Bonobos are also seen to go through four different mating strategies, such as promiscuous, restrictive, consortship, and extra-group mating in different situations. This is essentially done to maintain a good balance between the capabilities of the Bonobos and diversity in the community. These natural instincts of Bonobos were copied and mathematically expressed to solve an optimization problem in BO.

BO is a population-based method and it starts with a set of solutions created at random in the search space. It finds the alpha-bonobo, which is nothing but the best solution available in the current population in terms of fitness value. It also distinguishes two different phases, named as Positive phase (PP) and Negative phase (NP). In a PP, the fitness value of the alpha-bonobo is found to improve compared to its previous one. However, there is no improvement observed in the fitness of alpha-bonobo during a negative phase. Here, one adaptive parameter, namely phase-probability (p_p) is used to determine the phase during modification of any solution. According to the type of phase, the strategy for modifying a solution is selected. Moreover, in each phase, two types of modification strategies are used. However, in a PP, exploitation of the solutions is more focused, whereas exploration of the search space is become the prime concern during the NP. During the modification of each bonobo, one more solution, called as p^{th} -bonobo is selected using fission–fusion selection method for participating in mating. BO has five user-specific parameters, such as *scab* (sharing co-efficient for the alpha-bonobo), *scsb* (sharing co-efficient for the selected-bonobo or p^{th} -bonobo), *rcpp* (rate of change in phase-probability), $p_{xgm_initial}$ (initial probability of extra-group mating), and $tsgs_{factor_max}$ (maximum value of temporary sub-group size factor). Moreover, the controlling parameters of BO are designed to be adaptive in nature, so that the algorithm is become capable of managing a variety of situations with ease and efficiency. The source code of BO is obtained at: <https://in.mathworks.com/matlabcentral/fileexchange/104275-bonobo-optimizer-bo>.

3.2 Brief about NSGA-III

The basic structure of NSGA-III [34] is found to be the similar to that of NSGA-II [35]. However, there are significant differences in between them. In NSGA-III, a set of reference

points is created. It helps in maintaining a good balance between convergence and diversity of NSGA-III.

This many-objective optimization algorithm begins with an initial population of size N generated at random within the search space. It also creates M -dimensional reference points in the objective space and their positions are determined in the normalized hyper-plane using the method proposed by Das and Dennis [36]. For an M -objective problem ($M \geq 2$), the total number of reference points (H) to be generated is calculated as given in Eq. (1).

$$H = \binom{M + p - 1}{p} \quad (1)$$

where p is the number of divisions. The diversity in the population is maintained by a set of reference directions. In each reference direction, at least one solution is expected to be present. A reference direction may be seen as a ray, which begins from the origin point and passes through a reference point, as shown in Fig. 3.

Let us assume the parent population of size N at the t -th generation is denoted by P_t . Applying crossover and mutation, a children population (designated as Q_t) of size N is created from the parent ones. After combining the parent and children population, a mixed population (let's say C_t) of size $2N$ is obtained. This mixed population is then sorted into several non-domination ranks. From this population, a new population of size N is selected based on the assigned ranks and reference-direction based niching strategy. A flow-chart for NSGA-III is given in Fig. 4.

3.3 Regression analysis

Regression equation represents the dependency of output variable over the input variable represented on a scatter diagram. In the present study, the linear regression analysis was carried

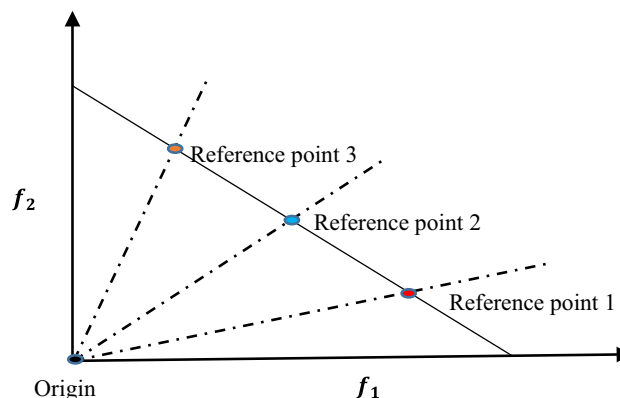


Fig. 3 On a normalized reference line, three reference points are given for an optimization problem with two-objectives

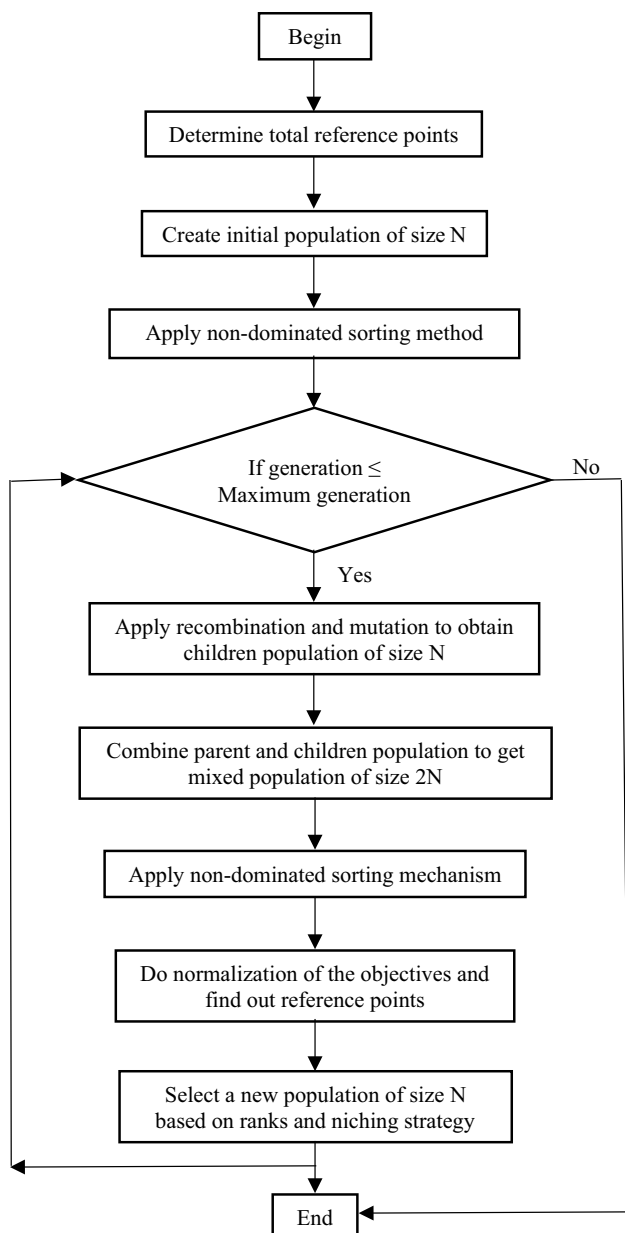


Fig. 4 Flowchart for NSGA-III

out. The direction of slope of line depends upon the relationship of input with the output. Here, Micro-hardness of FZ, yield strength, ultimate tensile strength and elongation dependency were expressed as the functions of duty cycle (D.C.), welding speed (S) and beam diameter (D), as given in Eqs. (2), (3), (4) and (5). The relationship of energy density with micro-hardness was negative, as there was decrease in hardness with the increase in the energy density, which can be interpreted from the slope of regression line which descends from left to right and presented in Fig. 5 (a). However, the regression line ascends from left to right for yield strength, ultimate tensile strength and elongation as shown in in Fig. 5 (b), (c) and

(d), which represents positive correlation. Figure 5 illustrates the trend of micro-hardness, yield strength, ultimate tensile strength and elongation with energy density. The R-squared value of each response was found to be closer to 1, which represents the suitable prediction capability of the developed equations. Figure 6 illustrates a comparison between experimental and predicted results. The predicted results of regression equations could closely follow the experimental results and the difference between the predicted and experimental results was acceptable.

The regression equations were obtained as follows:

$$FZ\ Hardness = 210.670 + 2.801 \times D.C. + 0.095 \times S - 103.360 \times D \quad (2)$$

$$R - S_q = 88.72\%$$

$$R-Sq = 88.72\%$$

$$UTS = 594.490 - 3.000 \times D.C. - 0.089 \times S - 15.530 \times D \quad (3)$$

$$R - S_q = 82.55$$

$$YS = 194.160 + 0.642 \times D.C. + 0.017 \times S - 58.980 \times D \quad (4)$$

$$R - S_q = 82.0\%$$

$$El = 22.500 - 0.183 \times D.C. - 0.005 \times S - 2.997 \times D \quad (5)$$

$$R - S_q = 80.3\%$$

3.4 Problem Formulation

A study was carried out for the optimization of the process parameters for laser welding. The input parameters were duty cycle (D.C.), welding speed (S) and beam diameter (D). The input parameters: duty cycle (D.C.) and welding speed (S) were of integer types and beam diameter (D) was a continuous variable with the rounded value up to the second decimal point. Moreover, duty cycle (D.C.) could take values in the range of (50, 70) with an interval of five. The many-objective optimization problem was formulated to maximize yield strength (YS), ultimate tensile strength (UTS), elongation (EL) and minimize the difference of micro-hardness (VHN) of the welded sample from that of the base-material, as given below in Eq. (6).

$$\begin{aligned} & \text{Maximize (YS, UTS, EL)} \\ & \text{and} \\ & \text{Minimize } |VHN - 108| \\ & \text{subject to } \begin{cases} 50 \leq D.C. \leq 70, \\ 600 \leq S \leq 1000, \\ 0.66 \leq D \leq 0.82, \end{cases} \end{aligned} \quad (6)$$

Fig. 5 Variations of (a) micro-hardness, (b) yield strength, (c) ultimate tensile strength, (d) elongation with energy density

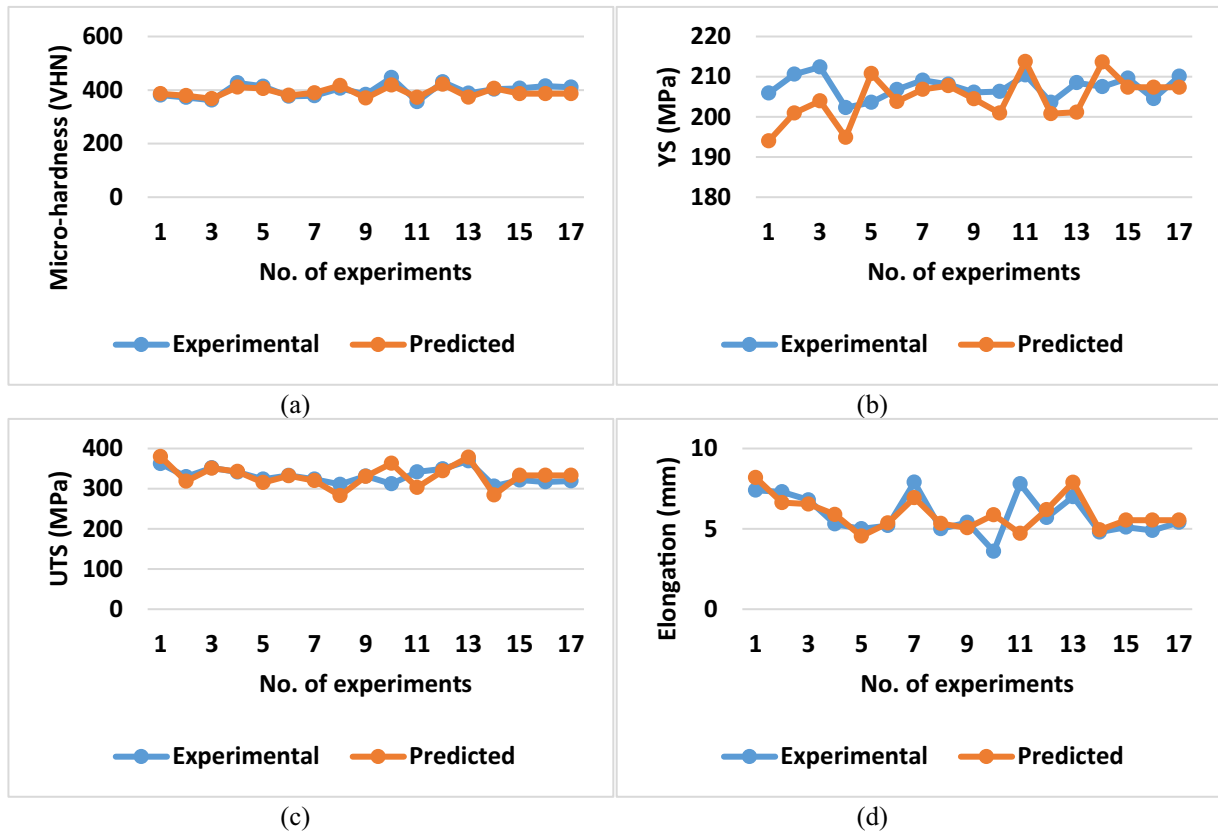
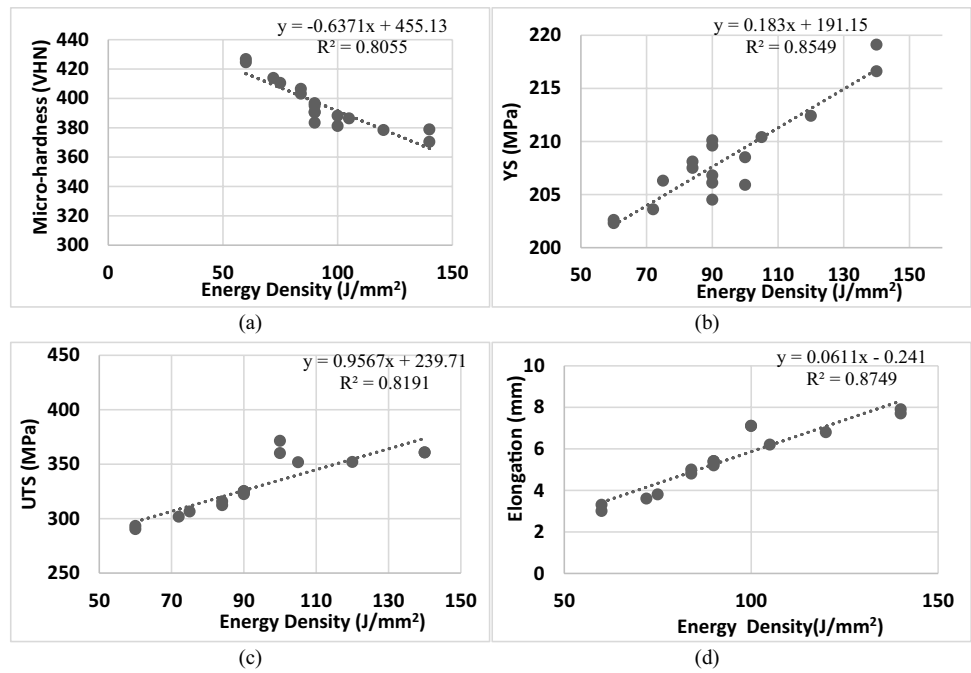


Fig. 6 Comparison between experimental and predicted results of (a) micro-hardness, (b) yield strength, (c) ultimate tensile strength, (d) elongation

where micro-hardness of the base-material (VHN_{BM}) was found to be equal to 108.

This many-objective optimization problem was solved using different approaches. The first method used for solving this problem was the traditional composite desirability approach (CDA). Then, the same problem was formulated as a single objective optimization one utilizing the weighted sum approach and solved using Bonobo Optimizer (BO). This many-objectives optimization problem was also solved using the evolutionary Non-dominated Sorting Genetic Algorithm (NSGA III), which was one of the recent and effective algorithms to handle many objectives.

4 Results

4.1 Results using composite desirability

Minitab was used to calculate the desirability for all the predicted responses. The desirability function is mainly of two types, that is, individual desirability, which assesses the variables used to optimize a single response and other is composite desirability that evaluates the variables to optimize more than one response. Composite desirability is the cumulative result of the values of the individual desirability and presents the relative emphasis of the responses. The desirability value presents how close the predicted result is to the target value. The optimal values of the parameters are identified and desirability value ranges from 0 to 1. If the value is found to be closer to 1, it signifies that desirability is high. Minitab due to default settings gives desirability value of 1 to each response in the problem. The value of desirability function informs how well the optimal parameters result into the desired responses. In the present study, the objectives were to obtain high strength (YS and UTS) and maximum elongation (El) and to minimize the micro-hardness (VHN) in the laser welded Nb-Zr-C alloy. Minitab helps in selecting input variables (D.C., S and D) to obtain the desirable responses. Figure 5 displays the variations of (a) micro-hardness, (b) yield strength, (c) ultimate tensile strength, (d) elongation with energy density. It is observed that there is decrease in the micro-hardness with increase in the energy density. Micro-hardness decreases due to the increase in the grain size, i.e., columnar grains. The welds having fine equiaxed grain have high hardness as compared to columnar grains which are observed in the welds joined using high energy density. The coefficient of determination (R^2) for micro-hardness with lie energy is 80.55%. The variation of yield strength, ultimate tensile strength and elongation presents an increasing trend with increase in energy density. The R^2 value of YS, UTS and elongation are 85.49%, 81.91% and 87.49% respectively. The correlation of property with energy density is significant. The

experimental and predicted results of (a) micro-hardness, (b) yield strength, (c) ultimate tensile strength, (d) elongation are compared in Fig. 6. The predicted values as obtained by composite desirability closely follows the experimental results. The variation of predicted results has a good agreement with the experimental results.

4.2 Results using BO and NSGA-III

Figure 7 showcases the results of the NSGA-III algorithm for the LBW problem using a 4-objective value path representation. The horizontal axis represents the four objectives, while the vertical axis displays their normalized values. This visualization allows for a comprehensive analysis of objective interrelationships and trade-offs. The distribution and density of points indicate the diversity of solutions and the achievement of balanced objectives. Normalized values on the vertical axis facilitate direct objective comparisons, aiding in trade-off identification and optimization analysis. The plot also highlights the Pareto-optimal solutions, that cannot be improved in all objectives simultaneously, providing insights for decision-making. In summary, Fig. 7 offers a valuable and concise representation of the LBW problem's many-objective optimization results using the NSGA-III algorithm.

At first single-objective optimization problem was solved by considering each one of the four objectives separately using BO. In the experiment, each problem was solved for a maximum of 100 iterations and the population size was kept equal to 30. The parameters of BO were selected using some trials and error method and these were found to be as follows: $scab = 1.25$, $susb = 1.3$, $rcpp = 0.0035$, $P_{xgm_initial} = 0.01$, and $tsgs_{factor_max} = 0.05$. In addition to this, the mentioned four objectives of the laser weld joints were

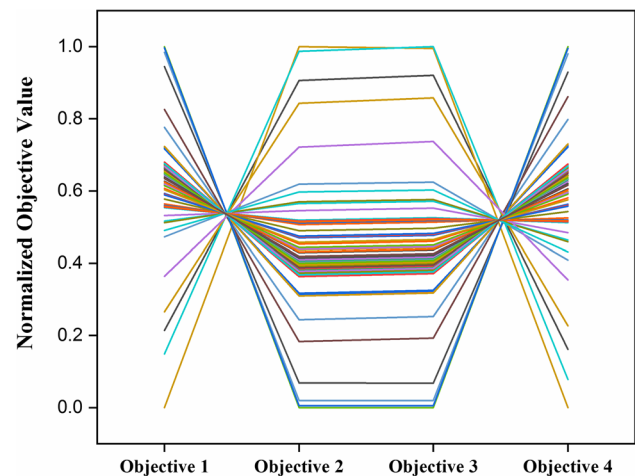


Fig. 7 NSGA-III solutions depicted using 4-objective value path for the LBW problem

combined together to convert the same into a single objective optimization utilizing the weighted sum approach. Here, equal weightage was provided to each of the four objectives and it was converted into a single objective optimization problem and solved using BO algorithm. The optimal solutions obtained using BO are reported in Table 5. It also contains the result of BO-tuned weighted sum approach. This many-objective optimization problem had also been solved using NSGA-III. Figure 7 depicts the value path plot of all yielded solutions for this problem with four objectives obtained using NSGA-III. Here, all the objectives had been represented using their normalized values in the range of (0, 1).

4.3 Confirmatory results of the meta-heuristic algorithms

The input parameters were optimized using the proposed meta-heuristic algorithms to obtain the desired results. The confirmation experiments were carried out using the different combinations of optimized input parameters. The different approaches used for optimization along with their predicted results and the corresponding experimental results are tabulated in Table 6. YS, UTS, EI and VHN are the desired results and YS (e), UTS (e), EI (e) and VHN (e) are the obtained experimental results through confirmatory tests. Figure 8 depicts the experimental results of stress vs. strain results yielded using different optimization algorithms. Figure 9 illustrates the variation of the micro-hardness of the confirmatory tests from the weld center-line towards the base metal obtained using different optimization techniques. BO-tuned weighted sum approach could yield the better performance compared to NSGA-III and composite desirability approach. Composite Desirability performed better than BO and NSGA-III in terms of percentage error calculated for yield strength (YS). However, BO-tuned method could yield 1.13%, 1.51% and 6.56% percentage deviation in micro-hardness (H.V), UTS and EI, which was in good agreement with the respective experimental results as shown in Table 7. BO-tuned weighted sum approach was found to be more accurate, which indicates its superiority compared to the

other algorithms used in this study. Therefore, in further texts comparison will be made with BO and welds joined with different heat-input.

4.4 Comparison of results of Bonobo optimizer with welds joined using different energy density

Corresponding to the input parameters yielded by BO, the input parameters identified was 50% D.C., 600 mm/min welding speed and beam diameter was 0.82 mm. BO suggested input parameters corresponds to energy density of 121.95 J/mm². From Table. 4 experiments 3 presents the input parameters for BO and experiment 2 and 16 presents input parameters for highest and lowest energy density. 73.17 J/mm² and 194.44 J/mm² corresponds to lowest and highest energy density used for welding as shown in Table 4. To evaluate the prominence of BO predicted results in terms mechanical and metallurgical properties, comparison of the cooling rate of corresponding energy density for BO and experiment 2 and 16 was carried out. Cooling rate controls the microstructural and metallurgical changes occurring in the FZ. Microstructural changes regulate the metallurgical and mechanical properties of the welded joints. Therefore, further study was based on the evaluating and comparing mechanical and metallurgical properties i.e., cooling rate, grain morphology, phase change, micro-hardness and tensile strength of 73.17 J/mm², 121.95 J/mm² and 194.44 J/mm².

In Fig. 10, curve AB depicts the heating cycle of the desired weld zone, when the laser beam and Infrared pyrometer spot coincides or overlaps. The descending curve BE is the cooling curve, as the laser advances away the spot of the pyrometer. The cooling curve can be divided into three distinct regions: BC, CD and DE, the region BC is the liquid or molten state that is marked as 'L'. Nucleation initiates from C above the melting point of 2470 °C, the nucleation sites are the un-melted zone or the HAZ. CD is the region, where both liquid and solid co-exists, 'S' signifies solid fraction of the molten pool. D is the temperature, at which whole molten-pool solidifies. The zone BD is the molten-pool life time of the experiment. The molten-pool thermal history has

Table 5 Obtained results of the single-objective problems using BO algorithm

Equation No	Objective function	Optimal parameters	Optimal objective value(s)
Equation (1)	Maximize YS	D.C. = 70, S = 1000, D = 0.66	YS = 217.800 MPa
Equation (2)	Maximize UTS	D.C. = 50, S = 600, D = 0.66	UTS = 379.890 MPa
Equation (3)	Maximize EL	D.C. = 50, S = 600, D = 0.66	EL = 8.104 mm
Equation (4)	Minimize VHN - 108	D.C. = 50, S = 600, D = 0.82	VHN = 323.780
Equation (5)	Minimize $0.25 * (\frac{1}{YS} + \frac{1}{UTS} + \frac{1}{EL} + VHN - 108)$	D.C. = 50, S = 600, D = 0.82	YS = 188.400 MPa, UTS = 377.410 MPa, EL = 7.624mm, VHN = 323.780

Table 6 Comparison of the experimental results of laser welding with that obtained using different optimization techniques

Approach	D.C.	S (mm/min)	D (mm)	YS (MPa)	YS(e) (MPa)	UTS (MPa)	UTS(e) (MPa)	EI (mm)	EI(e) (mm)	VHN	VHN(e)
NSGA-III	60	620	0.68	203.43	208.32	347.78	362.43	6.09	8.24	368.10	383.55
Composite Objective (BO)	50	600	0.82	208.40	212.80	377.41	371.71	7.62	7.12	323.78	286.57
Composite Desirability	50	1000	0.66	209.86	209.67	365.62	373.81	7.40	8.46	369.84	320.01

two solidification shelves due to alloying metal zirconium added to improve strength and resistance towards corrosion and oxidation.

Figure 11 presents the comparison of the thermal history of the experiments carried out at energy density of 73.17 J/mm², 121.95 J/mm² and 194.44 J/mm². The peak temperature of the experiments increases with the increase of the energy density. However, the cooling rate presents a decreasing trend with an increase of the energy density. The time required to solidify the molten pool is less for weld carried at low energy density as compared to the experiments carried at high energy density [37]. The experiments carried out at energy density of 73.17 J/mm² and 121.95 J/mm² had the same value of duty cycle, i.e., 50%, therefore, the controlling parameter for microstructural properties is the welding speed. However, the welding speed was kept constant and duty cycle and beam diameter was varied, when the comparison was done based on the properties of the weld carried out at energy density of 121.95 J/mm² and 194.44 J/mm². The increase in duty cycle could intensify the amount of energy density in localized area. Thus, the highest peak temperature occurred at the largest value of energy density per unit length. The effect of the cooling rate can be observed in Fig. 12, the grain size of the fusion zone decreased with the decrease in energy density. The grain morphology was found to be equi-axed, beaded shaped and trapezoidal for the energy density values of 73.17 J/mm², 121.95 J/mm² and 194.44 J/mm², respectively. The maximum temperature and cooling attained at different energy density are shown in Table 8. The joints welded at low energy density solidifies in between the laser pulses, due to high thermal conductivity of niobium and with the rise in temperature, the thermal conductivity increases during welding [38, 39].

4.4.1 Microstructure Analysis

The effect of energy density on grain size of the laser-welded samples could be analyzed by images of optical microscope, as shown in Fig. 12. The grain size refinement could be observed with a decrease in the energy density. High energy density resulted into the larger grains compared to that of the welds joined at the lower energy density. In Fig. 12(a), (b) and (c), the grains morphology changes from equi-axed to the beaded structure and then, epitaxial grain growth was observed, at the energy density of 73.13 J/mm², 121.95 J/mm² and 194.44 J/mm², respectively. The finer grains were observed at the lower energy density, since the extent of thermal gradient was of short duration, and with the increase in energy density, there was heat accumulation in the FZ, which resulted into the larger grains aligned along the thermal gradient. The larger grain in the center of the weld-bead was accommodated by sub-grains that generally was equiaxed in nature. The molten-pool's lifetime increased

Fig. 8 Stress vs. Strain results yielded by different optimization techniques

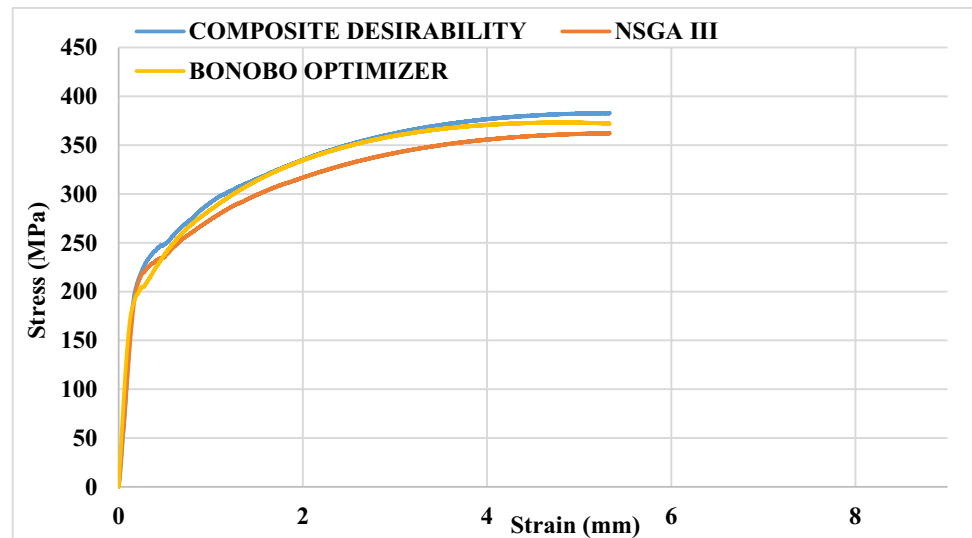
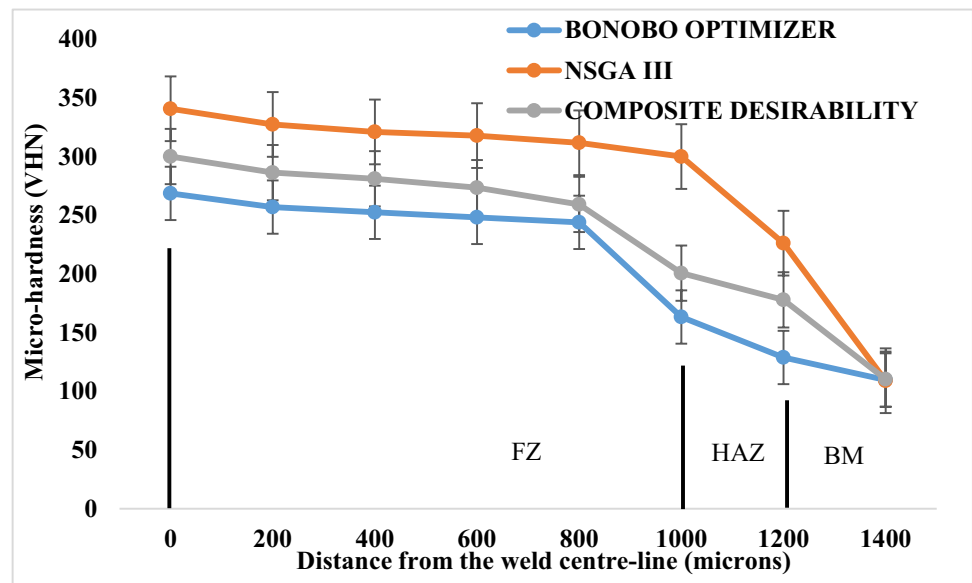


Fig. 9 Variations of micro-hardness from the weld centre-line towards the base metal obtained by different optimization techniques



with the energy density, and thereby resulted into FZ of the larger area of cross-section. The increase in energy density increased the temperature in the FZ, however, thermal conductivity of niobium decreases with temperature above 3000 K. The obtained maximum temperature increased with the increase in duty cycle, as shown in Table. 8. The solidification of molten pool occurred at the higher rate at low energy density due to high thermal conductivity, as compared to that of the higher energy density [38, 39].

4.4.2 Micro-hardness and phase analysis

The variation of the micro-hardness from the weld centre-line towards the base metal is presented in Fig. 13. The micro-hardness decreased, while measuring it from the weld

centre-line towards the base metal. The size of these sub-grains increased with an increase in energy density. Increase in hardness was also observed in the HAZ, as compared to the base metal [40, 41]. The highest values of micro-hardness observed at the weld centre-line were 455.8, 406.5 and 398.7 welded at energy density of 73.17 J/mm², 121.95 J/mm² and 194.44 J/mm², respectively.

The average micro-hardness values of the FZ were observed to be equal to 378.8, 388.1 and 426.5 for the energy density of 194.44 J/mm², 121.95 J/mm² and 73.17 J/mm², respectively, as shown in Fig. 14. The average micro-hardness presented a decreasing trend, as there is an increase of energy density, and this trend could be attributed to a decrease in cooling rate that ultimately decides the size of the grain in the FZ. Grain refinement is more at the lower

Table 7 Percentage error between experimental results for confirmatory tests of laser welding with that of forecast results using different optimization technique

Approach	YS (MPa)	YS(e) (MPa)	% Error	UTS (MPa)	UTS(e) (MPa)	% Error	El (mm)	El(e) (mm)	% Error	VHN	VHN(e)	% Error
NSGA-III	203.43	208.32	2.40	347.78	362.43	4.21	6.09	8.24	35.30	368.10	383.55	4.19
Composite Objective (BO)	208.40	212.80	2.11	377.41	371.71	1.51	7.62	7.12	6.56	383.78	388.15	1.13
Composite Desirability	209.86	209.67	0.09	365.62	373.81	2.24	7.40	8.46	14.32	369.84	320.01	13.47

energy density, as there is less time available for the grain growth during recrystallization from the molten state. The weld carried at the higher energy density has the larger grain size than that of the weld carried out at the lower energy density. Laser welding is popularly known for high cooling rate [42]. Moreover, niobium having high thermal conductivity aggravates the cooling phenomenon and therefore, energy density decides the hardness value attained by FZ post-solidification. Since, thermal conductivity of metal is temperature dependent property and niobium having high thermal conductivity aggravates the cooling phenomenon for the weld joined using energy density of 73.17 J/mm². However, it has been observed that thermal conductivity of niobium decreases with temperature after 2800 K (3073 °C) [39]. From Table.8 it can be concluded that the welds joined using energy density of 121.95 J/mm² and 194.44 J/mm² experienced fall in thermal conductivity and thus increase in molten-pool life time of the welds helped in grain growth at high energy density and therefore, heat energy density decides the hardness value attained by FZ post-solidification.

The X-ray diffraction analysis was done to study the phase changes occurring in the FZ after laser welding, as shown in Fig. 15. The observable change occurred in the formation of new carbides of niobium, such as Nb₆C₅ and NbC. The formation of carbides took place due to the dissolution of the unstable carbide precipitates occurring because of intense heat of the laser. The carbide phases of niobium, i.e., NbC formed in the FZ of all the welds, however, Nb₆C₅ occurred in the FZ of the joints carried out at energy density of 73.17 J/mm² due to increase in the welding speed and thermal conductivity, thereby high cooling rate, which was favorable for the formation of these phases. The high cooling rate did not allow the phase change from NbC to Nb₂C. Moreover, the presence of zirconium in the alloy facilitated the formation of the NbC in the FZ at the expense of Nb₂C. Nb₂C being an unstable phase acted as a preferential site for the diffusion of Zr. The diffusion of Zr into the carbide phase of niobium (α -Nb₂C) imparted instability to the phase. Ab-initio calculations approved the destabilization caused due to the presence of zirconium [43]. During solidification, stable phase of (Nb,Zr)C precipitates out at the expense of the Nb₂C phase. Gibb's free energy for the formation of ZrC, NbC and Nb₂C phases have demonstrated that (Nb,Zr)C carbide phase is more stable compared to Nb₂C in Nb-1%Zr-0.1%C alloy. The carbide phase of niobium, i.e., Nb₂C forms possibly at low temperature during the process of slow cooling. The formation of Nb₂C phase is suppressed by high cooling rate, which is favored by low heat-input [44]. The formation mechanism is given in Eq. (7)[43].

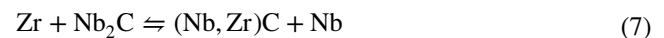


Fig. 10 Molten-pool thermal history depicting distinct phases of melting and solidification

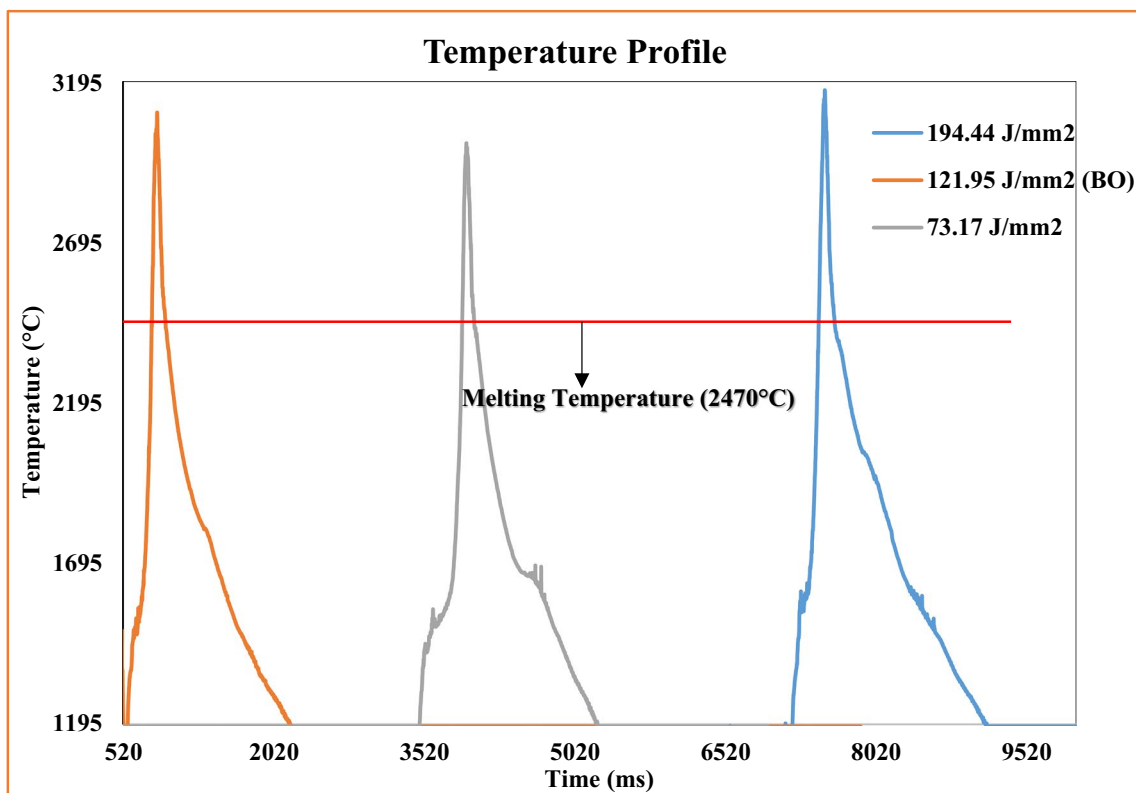
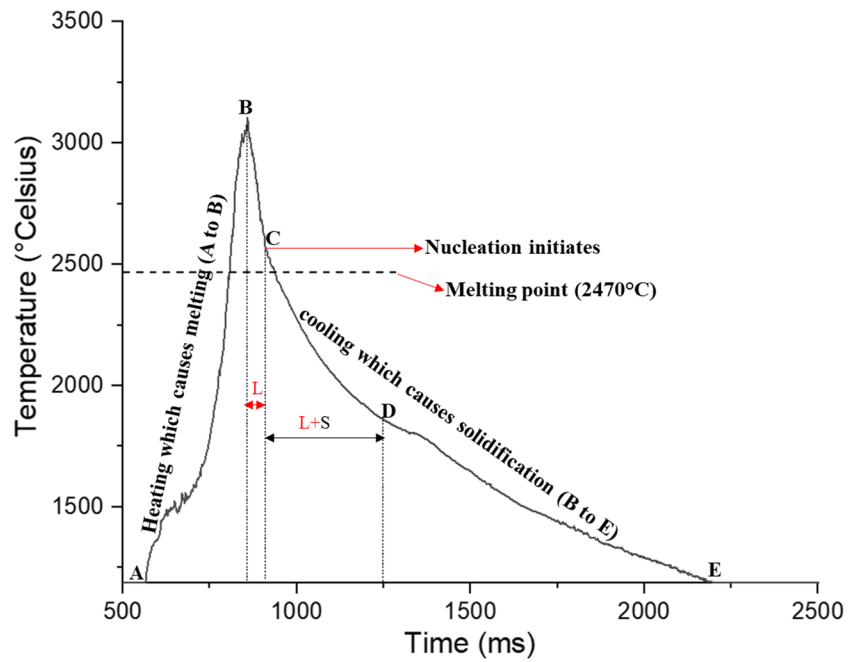


Fig. 11 Molten-pool thermal history of welds joined using energy density of 194.44 J/mm^2 , 121.95 J/mm^2 and 73.17 J/mm^2

4.4.3 Tensile test analysis

In the earlier studies, it was observed that welds of niobium

mostly failed in HAZ or FZ [17]. The evaluation of weld strength of laser-welded joints of niobium is required because an intense localized heat of laser causes detrimental

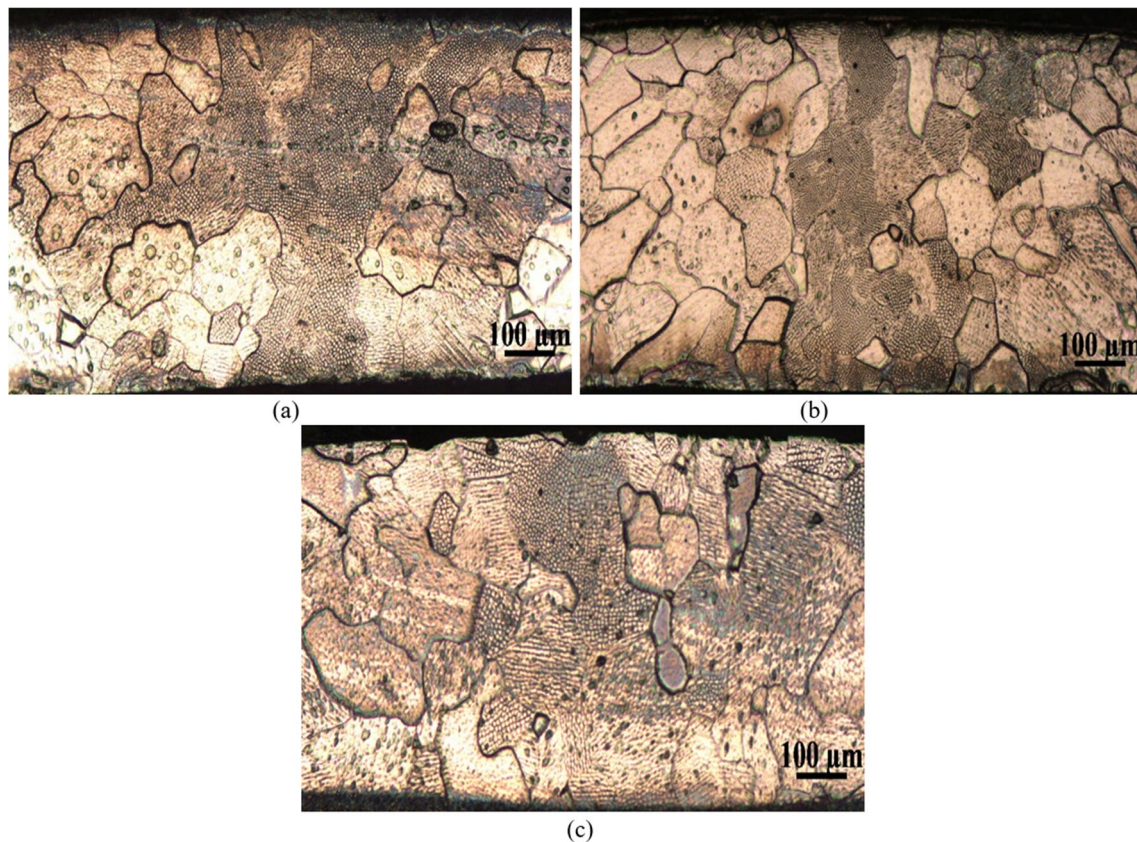


Fig. 12 Grain morphology obtained at energy density of (a) 73.17 J/mm² (b) 121.95 J/mm² (c) 194.44 J/mm²

Table 8 Maximum temperature and cooling rate for laser welding observed at different energy density

Energy density (J/mm ²)	Maximum Temperature (°C)	Cooling Rate (°C/s)
73.17	3007.2	3011.3
121.95 (BO)	3102.6	2609.1
194.44	3172.4	2081.0

change in the weld. The degradation of mechanical and metallurgical properties of the weld joints can be studied by assessment of tensile strength, micro-hardness and micro-structure. Uniaxial tensile test of the laser welded sample was carried out to find the yield strength, tensile strength and elongation of the joints. High cooling rate is characteristics of the laser welding, which is evident from the molten pool's lifetime measured in milli-seconds. Inert gas is suggested for shielding of the weld zone of highly reactive metals, such as niobium. Optimization of flow of shielding gas is required to maintain a proper balance between cooling rate and availability of inert environment around the weld zone. The strength and ductility of the welded joints were quantified by uniaxial tests. From Fig. 16, it is evident that strength

(YS and UTS) and plasticity of the joints improved with the increase in the energy density of the joints. The area under stress–strain curve of the welded joints explains the deformation incurred by the joints before failure. The decrease in the strength, i.e., yield strength and ultimate tensile strength could be attributed to the molten-pool's thermal history that determines the grain size and micro-hardness. The welded joints presented grain refinement with the decrease in energy density due to an increase in the welding speed, i.e., cooling rate. The grain size refinement resulted into an increment of micro-hardness of the joints. Increment of micro-hardness further escalates the chances of brittle fracture. Grain with small area could accommodate a smaller number of dislocations during the uni-axial test. Grain boundary could impede the movement of the dislocation, therefore, dislocation piling up occurred at the grain boundary. When the threshold of the stacking of the dislocation was reached, the failure got initiated by crack formation. The threshold was determined by the strength of the grain boundary.

Nb-Zr-C welds were susceptible towards loss of strength and plastic deformation, when joined to attain full-penetration welds using laser. High thermal conductivity and melting point of niobium necessitate the use of high energy density for fabrication. Figure 17 presents the fracture surface

Fig. 13 Variations of micro-hardness from the weld centre-line towards the base metal for the welds joined using energy density of 194.44 J/mm^2 , 121.95 J/mm^2 and 73.17 J/mm^2 .

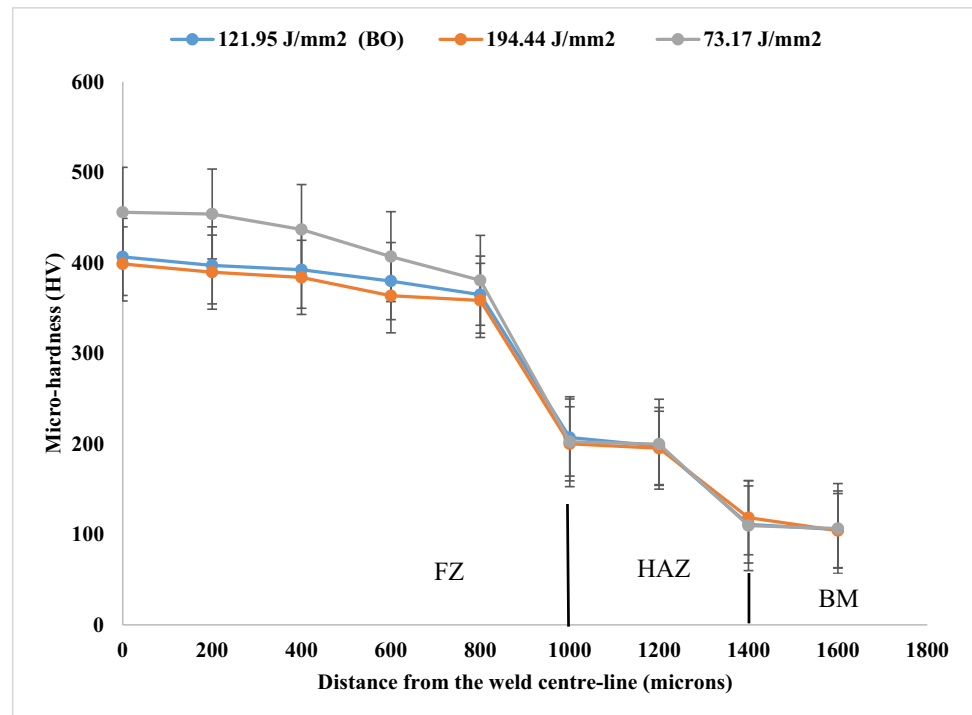
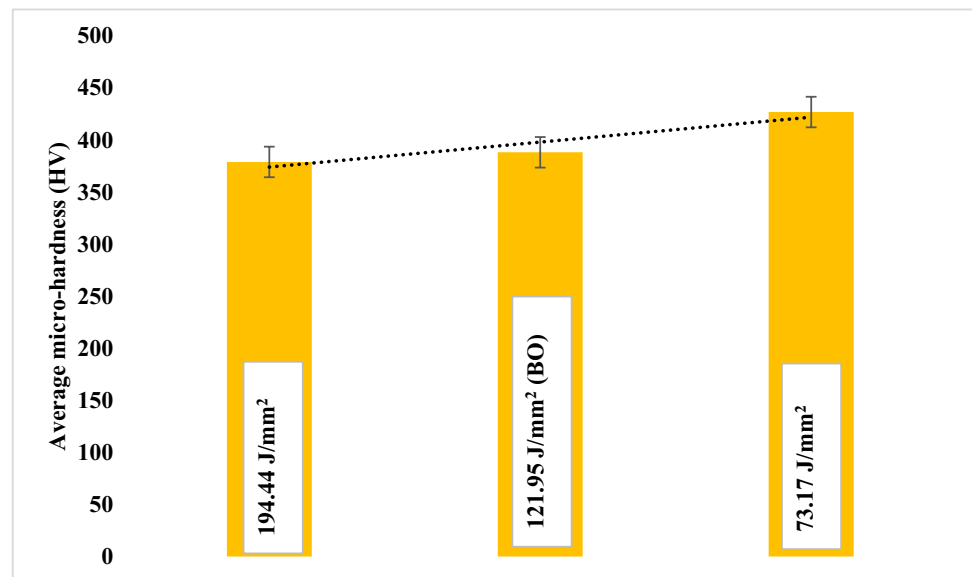


Fig. 14 Average micro-hardness for the welds joined using energy density of 194.44 J/mm^2 , 121.95 J/mm^2 and 73.17 J/mm^2 .



of welds obtained using energy density of (a) 194.44 J/mm^2 (b) 121.95 J/mm^2 and (c) 73.17 J/mm^2 . These dimples, as observed in Fig. 17 (a) and (b) are the spherical micro-voids that acts as the centre point for the initiation of the crack. The extent of ductility can be interpreted by analyzing the size of the dimples. Since the welds of 194.44 J/mm^2 and 121.95 J/mm^2 have difference in ductility of 0.8 mm, the difference in dimple size reflects the variation in elongation achieved during uni-axial tests. The size of the dimple signifies the extent of plasticity a sample has endured,

before the failure or fracture occurs. The fractured surface of the welded samples with the energy density of 73.17 J/mm^2 presented trans-granular mode of fracture. The brittle fracture occurs due to sudden drop of load as depicted in Fig. 16. Figure 18 depicts the fracture location sites of the welds where the encircled region indicate the location of the failure. The fracture location of the welds of 194.44 J/mm^2 and 121.95 J/mm^2 are located in the base metal whereas the fracture location if the weld of 73.17 J/mm^2 is located in the FZ. The difference in the average micro-hardness of

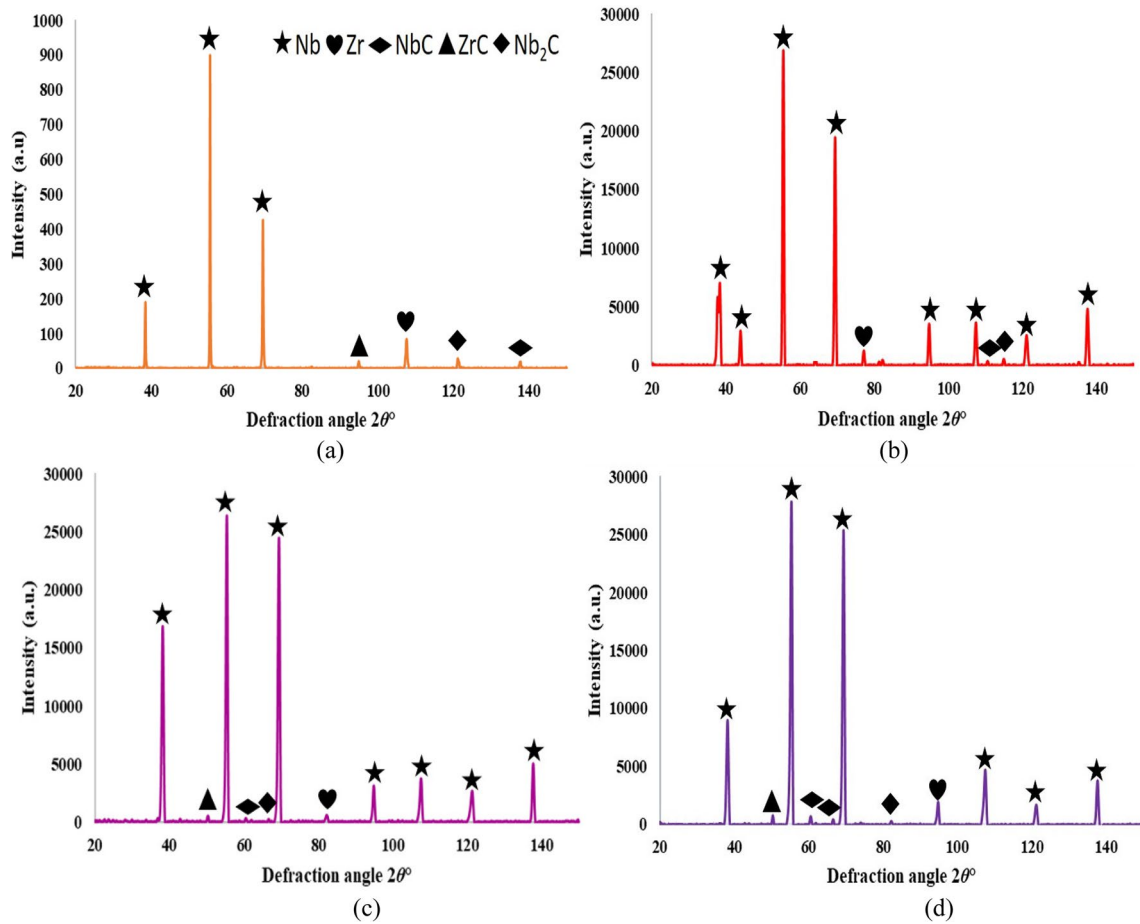


Fig. 15 XRD phase analysis of welds joined using energy density of (a) base metal (b) 73.17 J/mm² (c) 121.95 J/mm² (d) 194.44 J/mm²

Fig. 16 Stress v/s strain for welds joined using energy density of 194.44 J/mm², 121.95 J/mm² and 73.17 J/mm²

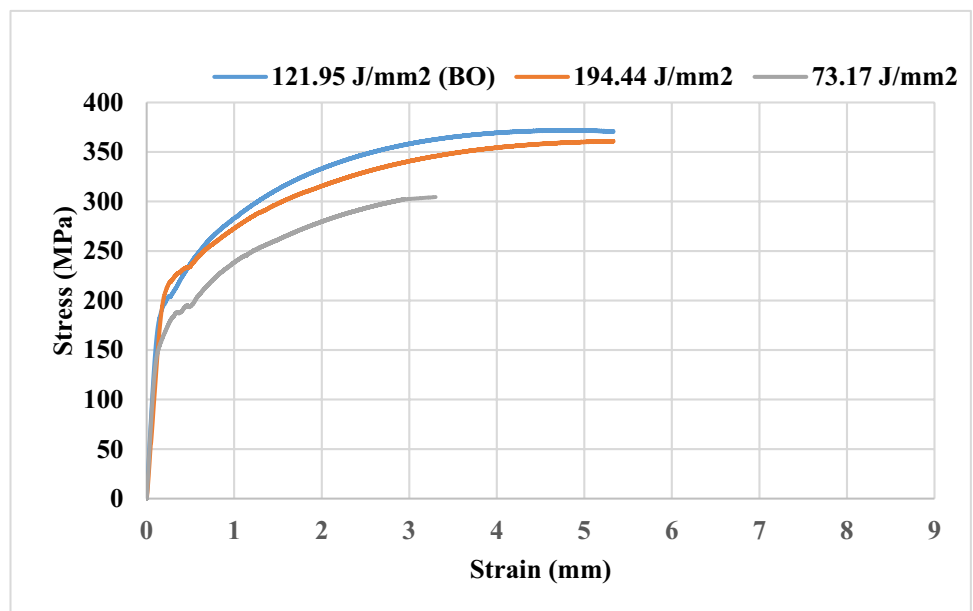
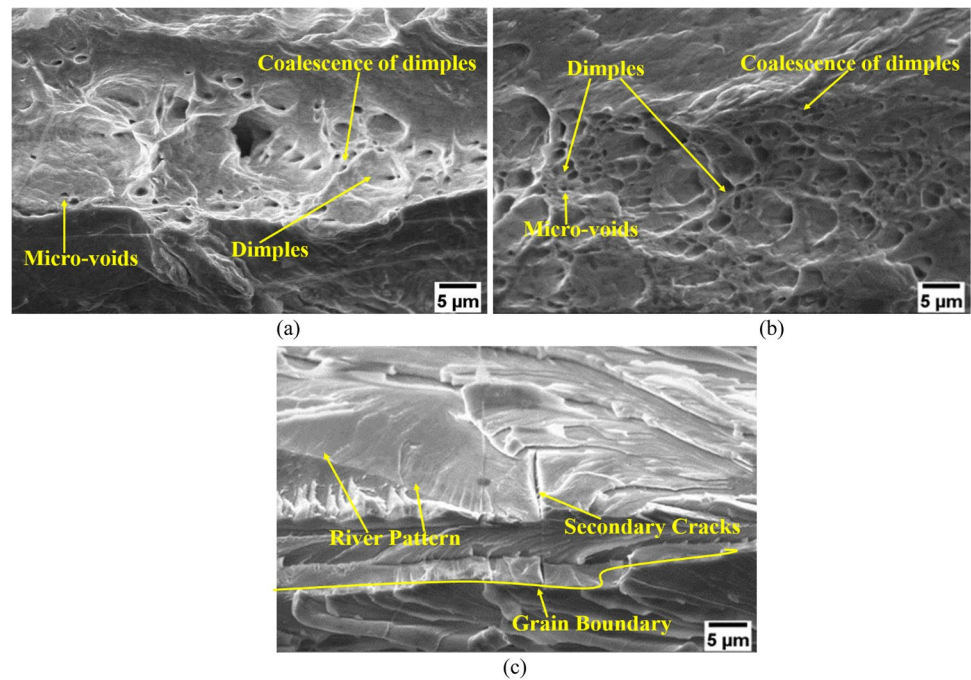


Fig. 17 Fracture surface of welds joined using energy density of (a) 194.44 J/mm² (b) 121.95 J/mm² and (c) 73.17 J/mm²



the welds of 194.44 J/mm² and 121.95 J/mm² is 9.3 H.V. Therefore, the fracture sites are located in BM and both the samples presents ductile mode of failure during uni-axial tensile test which is confirmed by the analysis of fracture surface as shown in Fig. 17. The FZ of the weld 73.17 J/mm² consists of small equi-axed grains whereas the welds of 194.44 J/mm² and 121.95 J/mm² consists of equi-axed grains in the centre of FZ, large beaded grains and elongated or trapezoidal grains at the interface of FZ and HAZ. These elongated grains helped in the plasticity. Hence, microstructure and micro-hardness, which are controlled by cooling

rate and energy density, influence the tensile strength and ductility of the weld metals.

5 Discussion

Energy density determines the molten-pool history and overall, controls the mechanical and metallurgical properties of the welded joints. Laser being high intensity power source for joining of the alloy, the probability of dynamic recrystallization and grain refinement in FZ will result into the

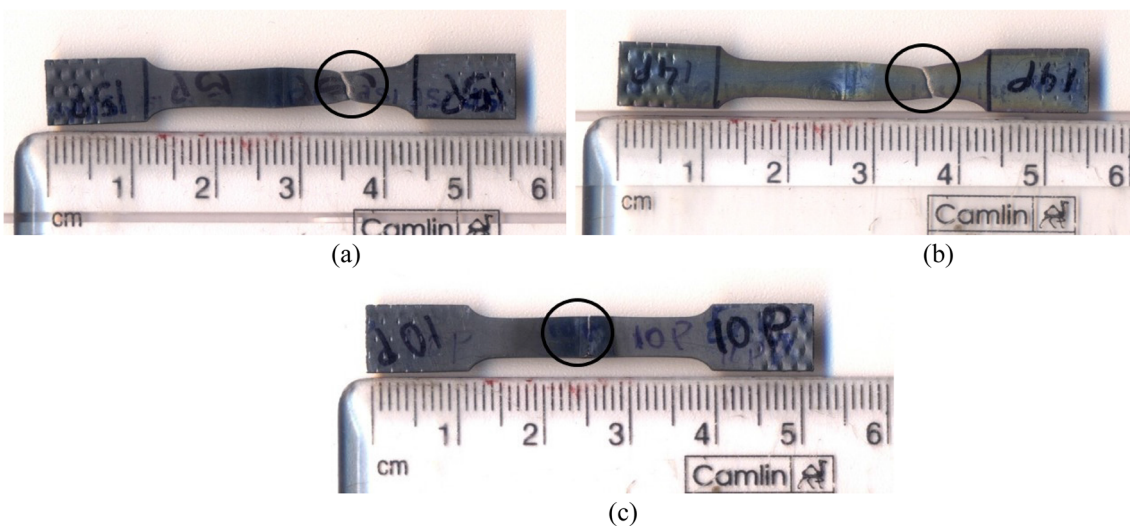


Fig. 18 Location of fracture sites of welds joined using energy density of (a) 194.44 J/mm² (b) 121.95 J/mm² and (c) 73.17 J/mm²

change of mechanical and metallurgical properties. Increase in hardness of joints can be primarily attributed to grain size. The center of the FZ of the welded samples is composed of the fine equi-axed grains. The equi-axed grains size varies from 1 to 2 μm . Beaded shaped grains could be observed adjacent to the equi-axed grains in the FZ. These micro-features vary between 10 and 15 μm , and lamellar structures having the size of 20–22 μm are generally located at the transition zone of FZ to HAZ. The lamellar structures significantly contribute in the plastic deformation during tensile tests. There is a gradual increase in the grain size from centre of the FZ towards the BM, the increase in grain size is reflected on the micro-hardness of the FZ. Increase in grain size results into a decrease in the micro-hardness. The ultimate tensile strength of the joints was found to increase with the increase in the energy density. The lowest strength and ductility were observed for the weld joined at 73.17 J/mm². The welded joint obtained using the optimized parameters yielded by Bonobo Optimizer, i.e., at 121.95 J/mm² could perform better compared to the weld joint with 194.44 J/mm². The yield strength of the welded joint obtained using 121.95 J/mm² matches with that of the same at 194.44 J/mm². The ultimate tensile strength of the weld of 121.95 J/mm² was found to be more compared as to that yielded 194.44 J/mm², and the difference in their ultimate tensile strength was 10.91 MPa. The elongations obtained for the energy density of 73.17 J/mm², 121.95 J/mm² and 194.44 J/mm² were 3.28 mm, 7.11 mm and 7.93 mm, respectively. The values of percentage of elongation were seen to be equal to 29.41%, 64.05% and 71.44% in comparison with base metal. Ductility and percentage elongation of the weld joined at 121.95 J/mm² were less as compared to that yielded at 194.44 J/mm². The difference in plastic deformation and percentage elongation could be attributed to grain morphology. Therefore, elongation and strength could be maximized by controlling the cooling rate and evolution of microstructure. The ductility in the samples improves due to the formation and coalescence of dimples. The larger voids are formed due to the coalescence of dimples. The size of these voids gets reflected on the ductility of the samples. Overall, Bonobo optimizer almost conforms to mechanical and metallurgical properties of the weld joined using the highest heat input. Hence, Bonobo optimizer suits for solving the present many-objective optimization problem.

6 Conclusion

Pulsed laser welding of Nb-Zr-C alloy had been conducted to optimize the process parameters in order to obtain maximum joint strength, ductility and a desirable hardness in the joint. The many objectives optimization problem had been solved using traditional composite desirability approach, Bonobo

optimizer-tuned weighted sum approach and metaheuristic NSGA-III algorithms.

1. Bonobo optimizer-based weighted sum approach with the least value of mean absolute deviation seems to be more efficient in predicting the optimized result among all algorithms because of adaptive nature of BO in terms of parameter handling. A pulsed laser beam diameter of 0.82 mm with a scanning speed of 600 mm/min and duty cycle of 50% was found to be the optimized parameters for maximizing the strength and ductility. The weld joint fabricated using the input parameters or corresponding energy density as yielded by bonobo optimizer almost conforms the mechanical and metallurgical properties of the weld joined using highest heat input.
2. The micro-hardness, yield strength, ultimate tensile strength and elongation of the weld were observed to be dependent on the energy density. UTS value of the optimized combinations almost reached as that of the parent alloy. However, there was reduction of yield strength and elongation in the optimized combination as compared to the base metal. This could be due to the significant enhancement of hardness in weld due to grain refinement.
3. The average hardness for the optimized weld joint was almost four times of that of the parent material's hardness. Inherent high cooling rate of laser welding, high thermal conductivity of Nb-Zr-C alloy and grain structure evolution during the post-solidification of welding could be the possible reasons for the aggravated result of micro-hardness in FZ.
4. The pulsed welded joint of Nb-Zr-C alloy exhibit the higher strength and elongation with reduction of grain refinement. Trapezoidal grains presented maximum strength and elongation as compared to equi-axed and beaded grains. This phenomenon could be attributed by the enhancement of molten pool's life time and decrease in cooling rate with the increase of energy density.

Declarations

Conflict of interest The author declares that there exists no competing financial interest or personal relationships that could have appeared to influence the work reported in this paper.

References

1. Jaypuria S, Kumar Gupta S, Suresh-Fazeela S (2019) Study of metallurgical and mechanical behavior of laser butt-welded dissimilar joint of inconel and stainless steel. ASME Int Mech Eng Congr Expo Proc. <https://doi.org/10.1115/IMECE2019-12238>

2. Poggie RA, Kovacs P, Davidson JA (1996) Oxygen diffusion hardening of Ti-Nb-Zr alloys. *Mater Manuf Process* 11:185–197. <https://doi.org/10.1080/10426919608947472>
3. Bewlay BP, Jackson MR, Zhao J, Subramanian PR (2003) A Review of Very-High-Temperature Nb-Silicide – Based Composites. *Metall and Mater Trans A* 34:2043–2052. <https://doi.org/10.1007/s11661-003-0269-8>
4. Maldonado J, Kangilaski M, Ring PJ (1994) PWC-11 fabrication methods for optimum strength for SP-100 applications. 11th Symp Sp Nucl Power Propulsion. *AIP Conf Proc* 301:1347–1352. <https://doi.org/10.1063/1.2950146>
5. da Costa AR, Craievich A, Vilar R (2004) Niobium and chromium rich coatings tailored by laser alloying: XRD analysis at high temperatures. *Mater Res* 7:49–52. <https://doi.org/10.1590/S1516-14392004000100008>
6. Chaudhuri A, Sarkar A, Kapoor R (2014) Microstructural Features of Hot Deformed Nb-1Zr-0.1C Alloy. *Jom* 66:1923–1929. <https://doi.org/10.1007/s11837-014-1122-9>
7. Vishwanadh B, Vaibhav K, Jha SK (2012) Development of Nb – 1 % Zr – 0. 1 % C alloy as structural components for high temperature reactors. *J Nucl Mater* 427:350–358. <https://doi.org/10.1016/j.jnucmat.2012.04.014>
8. Dulera IV, Sinha RK, Rama Rao A, Patel RJ (2017) High temperature reactor technology development in India. *Prog Nucl Energy* 101:82–99. <https://doi.org/10.1016/j.pnucene.2017.04.020>
9. Gao XL, Liu H, Liu J, Yu H (2019) Laser welding of Ti6Al4V to Cu using a niobium interlayer. *J Mater Process Technol* 270:293–305. <https://doi.org/10.1016/j.jmatprotec.2019.03.005>
10. Torkamany MJ, MalekGhaini F, Poursalehi R (2014) Dissimilar pulsed Nd: YAG laser welding of pure niobium to Ti-6Al-4V. *Mater Des* 53:915–920. <https://doi.org/10.1016/j.matdes.2013.07.094>
11. Hajitabar A, Naffakh-Moosavy H (2018) Effect of electron beam welding current variations on the microstructure and mechanical properties of Nb-1Zr advanced alloy. *Vacuum* 150:196–202. <https://doi.org/10.1016/j.vacuum.2018.01.043>
12. Badgajar BP, Kumar S, Jha MN (2017) An investigation of electron beam welding of Nb-1Zr-0.1C alloy: Process parameters and microstructural analysis. *J Manuf Process* 28:326–335. <https://doi.org/10.1016/j.jmapro.2017.07.001>
13. Titran RH, Moore TJ, Grobstein TL (1986) Creep properties of PWC-11 base metal and weldments as affected by heat treatment. *NASA Tech Memo* 88842:1–22. <https://www.osti.gov/servlets/purl/10181379>
14. Franchini F, Pierantozzi P (1992) Electron beam welding of dissimilar materials: Niobium-base alloy C-103 with titanium-base alloy Ti-6Al-4V ELI. *Weld Int* 6:792–797. <https://doi.org/10.1080/09507119209548287>
15. Hirose H, Sato K, Hayashi T (1989) Welding of tantalum and niobium. *Weld Int* 3:672–677. <https://doi.org/10.1080/09507118909446635>
16. Scott MH, Knowlson PM (1963) The welding and brazing of the refractory metals niobium, tantalum, molybdenum and tungsten-A Review. *J Less-Common Metals* 5:205–244. [https://doi.org/10.1016/0022-5088\(63\)90029-8](https://doi.org/10.1016/0022-5088(63)90029-8)
17. Kramer D, McDougal J, Booher B (2000) Electron beam and Nd-YAG laser welding of niobium-1 percent zirconium and molybdenum-44.5 percent rhenium thin sheet material. 35th Intersoc Energy Convers Eng Conf Exhib 2:956–961. <https://doi.org/10.2514/6.2000-2971>
18. Saha P, Waghmare D (2020) Parametric optimization for autogenous butt laser welding of sub-millimeter thick SS 316 sheets using central composite design. *Opt Laser Technol* 122:105833. <https://doi.org/10.1016/j.optlastec.2019.105833>
19. Kanigalpula PKC, Jaypuria S, Pratihari DK, Jha MN (2018) Experimental investigations, input-output modeling, and optimization of spiking phenomenon in electron beam welding of ETP copper plates. *Meas J Int Meas Confed* 129:302–318. <https://doi.org/10.1016/j.measurement.2018.07.040>
20. Heydari H, Akbari M (2020) Investigating the effect of process parameters on the temperature field and mechanical properties in pulsed laser welding of Ti6Al4V alloy sheet using response surface methodology. *Infrared Phys Technol* 106:103267. <https://doi.org/10.1016/j.infrared.2020.103267>
21. Jaypuria S, Gupta SK, Pratihari DK (2020) Comparative Study of Feed-Forward and Recurrent Neural Networks in Modeling of Electron Beam Welding 521–531. https://doi.org/10.1007/978-981-32-9433-2_45
22. Liu G, Gao X, Peng C (2020) Optimization of laser welding of DP780 to Al5052 joints for weld width and lap-shear force using response surface methodology. *Opt Laser Technol* 126:106072. <https://doi.org/10.1016/j.optlastec.2020.106072>
23. Jaypuria S, Mahapatra TR, Tripathy S (2020) Fuzzy C-means Clustering-Based ANFIS Regression Modeling of Hybrid Laser-TIG Fabrication 617–624. https://doi.org/10.1007/978-981-15-1307-7_70
24. Jaypuria S, Mahapatra TR, Sahoo S, Jaypuria O (2019) Computational intelligence based prediction of joint penetration in laser fabrication. *Mater Today Proc* 46:4854–4858. <https://doi.org/10.1016/j.matpr.2020.10.325>
25. Jaypuria S, Das AK, Pratihari DK (2018) Swarm-Intelligence-Based Computation for Parametric Optimization of Electron Beam Fabrication. *Adv Comput Methods Manuf* 153–163. https://doi.org/10.1007/978-981-32-9072-3_14
26. Das D, Jaypuria S, Pratihari DK, Roy GG (2021) Weld optimisation. *Sci Technol Weld Join* 26:181–195. <https://doi.org/10.1080/13621718.2021.1872856>
27. Shah K, Kumar R, Sahoo S (2017) Optimization of annealing cycle parameters of dual phase and interstitial free steels by multiobjective genetic algorithms. *Mater Manuf Process* 32:1201–1208. <https://doi.org/10.1080/10426914.2016.1257134>
28. Bal KS, Nair AM, Dey D, Singh AK, Choudhury AR (2018) Multi-objective Optimisation of Electro Jet Drilling Process Parameters for Machining of Crater in High-Speed Steel Using Grey Relational Analysis. *Adv Unconvent Mach Compos* 385–395. https://doi.org/10.1007/978-981-32-9471-4_31
29. Singh AK, Bal KS, Dey D (2021) Experimental investigation and parametric optimization for minimization of dilution during direct laser metal deposition of tungsten carbide and cobalt powder mixture on SS304 substrate. *Powder Technol* 390:339–353. <https://doi.org/10.1016/j.powtec.2021.05.056>
30. Seada H, Deb K (2015) U-NSGA-III: A Unified Evolutionary Optimization Procedure for Single, Multiple, and Many Objectives: Proof-of-Principle Results. *Lecture Notes in Computer Science (Lecture Notes in Artificial Intelligence and Lecture Notes in Bioinformatics)* 34–49. https://doi.org/10.1007/978-3-319-15892-1_3
31. Li C, Huang J, Wang K (2019) Optimization of processing parameters of laser skin welding in vitro combining the response surface methodology with NSGA- II. *Infrared Phys Technol* 103:103067. <https://doi.org/10.1016/j.infrared.2019.103067>
32. Pérez Medina GY, CarrumSiller EG, Miranda Pérez AF, Saldaña-Garcés R (2019) Mechanical Properties and Depth Penetration Optimization Using NSGA-III in Hybrid Laser Arc Welding. *MRS Adv* 4:3053–3060. <https://doi.org/10.1557/adv.2019.364>
33. Das AK, Pratihari DK (2021) Bonobo optimizer (BO): an intelligent heuristic with self-adjusting parameters over continuous spaces and its applications to engineering problems. *Appl Intell* 52:2942–2974. <https://doi.org/10.1007/s10489-021-02444-w>
34. Deb K, Jain H (2014) An evolutionary many-objective optimization algorithm using reference-point-based nondominated sorting approach, Part I: Solving problems with box constraints. *IEEE*

- Trans Evol Comput 18:577–601. <https://doi.org/10.1109/TEVC.2013.2281535>
35. Deb K, Pratap A, Agarwal S, Meyarivan T (2002) A fast and elitist multiobjective genetic algorithm: NSGA-II. *IEEE Trans Evol Comput* 6:182–197. <https://doi.org/10.1109/4235.996017>
 36. Das I, Dennis JE (1998) Normal-Boundary Intersection: A New Method for Generating the Pareto Surface in Nonlinear Multicriteria Optimization Problems. *SIAM J Optim* 8:631–657. <https://doi.org/10.1137/S1052623496307510>
 37. Gupta SK, Pal PK (2018) Analysis of through transmission laser welding of Nylon6 by finite element simulation. *Manag Prod Eng Rev* 9:56–69. <https://doi.org/10.24425/119546>
 38. Torkamany MJ, MalekGhaini F, Poursalehi R, Kaplan AFH (2016) Combination of laser keyhole and conduction welding: Dissimilar laser welding of niobium and Ti-6Al-4V. *Opt Lasers Eng* 79:9–15. <https://doi.org/10.1016/j.optlaseng.2015.11.001>
 39. Singaravelu S, Klopff JM, Krafft G, Kelley MJ (2011) Laser nitriding of niobium for application to superconducting radio-frequency accelerator cavities. *J Vac Sci Technol B, Nanotechnol Microelectron Mater Process Meas Phenom* 29:061803. <https://doi.org/10.1116/1.3656380>
 40. Gupta SK, Datta S, Jaypuria S, Pratihari DK, Saha P (2020) A Critical Study of Bead-on-Plate Laser Welding of Niobium Alloy PWC-11 397–404. https://doi.org/10.1007/978-981-15-1307-7_44
 41. Gupta SK, Jaypuria S, Pratihari DK, Saha P (2021) Experimental Investigation on Microstructure and Mechanical Properties of Laser-Welded Nb-1% Zr-0.1% C Alloy. *J Mater Eng Perform* 30:8412–8425. <https://doi.org/10.1007/s11665-021-05979-8>
 42. Bal KS, Dutta Majumdar J, Roy Choudhury A (2019) Optimization of Melt Zone Area for Electron Beam Welded Hastelloy C-276 Sheet and Study of Corrosion Resistance of the Optimized Melt Zone in 3.5 wt% NaCl Aqueous Solution. *Arab J Sci Eng* 44:1617–1630. <https://doi.org/10.1007/s13369-018-3629-9>
 43. Vishwanadh B, Arya A, Tewari R, Dey GK (2018) Formation mechanism of stable NbC carbide phase in Nb-1Zr-0.1C (wt.%) alloy. *Acta Mater* 144:470–483. <https://doi.org/10.1016/j.actamat.2017.11.007>
 44. Ostermann F, Kibbey EE, Ostermann F (1970) Molybdenum in Nb-C Alloys. *Metallurgical Transactions* 1:2257–2263. <https://doi.org/10.1007/BF02643443>
- Publisher's Note** Springer Nature remains neutral with regard to jurisdictional claims in published maps and institutional affiliations.
- Springer Nature or its licensor (e.g. a society or other partner) holds exclusive rights to this article under a publishing agreement with the author(s) or other rightsholder(s); author self-archiving of the accepted manuscript version of this article is solely governed by the terms of such publishing agreement and applicable law.